Detection of laser driven deuterium ions by employing differentially filtered image plate detectors in Thomson spectrometers

Contact: aalejo01@qub.ac.uk

A. Alejo, S. Kar, H. Ahmed, D. Doria, A. Green, D. Jung, C.L.S. Lewis, G. Nersisyan, M. Zepf, M. Borghesi
Centre for Plasma Physics, School of Mathematics and Physics, Queen's University Belfast, BT7 1NN, UK

A.G. Krygier, R.R. Freeman
Department of Physics, The Ohio State University, Columbus, Ohio 43210, USA

J.T. Morrison
Propulsion Systems Directorate, Air Force Research Lab, Wright Patterson Air Force Base, Ohio 45433, USA

R. Clarke, J.S. Green, P. Norreys*, M. Notley
†*Central Laser Facility, Rutherford Appleton Laboratory, Didcot, Oxfordshire, OX11 0QX, UK*

M. Oliver
**Department of Physics, University of Oxford, Oxford, OX1 3PU, UK*

J. Fuchs, L. Vassura
LULI, Ecole Polytechnique, CNRS, Palaiseau Cedex, 91128, France

J. Fernández†, J.A. Ruiz
Instituto de Fusión Nuclear, Universidad Politécnica de Madrid, Madrid, 28006, Spain

A. Kleinschmidt, M. Roth
Institut für Kernphysik, Technische Universität Darmstadt, Schloßgartenstrasse 9, D-64289 Darmstadt, Germany

Z. Najmudin, H. Nakamura
Blackett Laboratory, Department of Physics, Imperial College London, SW7 2AZ, UK

1 Introduction

One of the diagnostics commonly used to characterize the high power laser driven multispeies ion beams is the Thomson Parabola Spectrometer (TPS)[1, 2], which has the unique ability to retrieve the ion spectra for species with different charge-to-mass ratio.

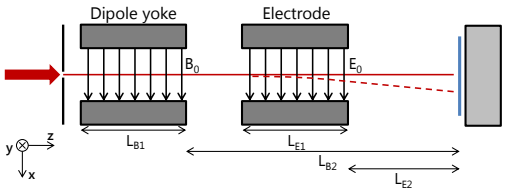

Figure 1: Schematic of a typical TPS with regions of static magnetic and electric fields.

In a typical TPS (Fig. 1), a pencil beam of ions, selected by the pinhole located at its entrance, travels through regions of parallel magnetic and electric fields, applied transversely to the beam axis, before reaching the detector plane. With reference to fig. 1, the magnetic field determines the position of the ions along the y-axis, depending on their energy per nucleon (W) (or longitudinal velocity (v_z)), while the electric field deflects the ions along the the x axis according to their charge (q) to mass (m) ratio. Assuming that the inhomogeneities of the fields are negligible and that the ion energies are not relativistic, particles with given q/m will lay on a parabolic trace on the detector plane described by the expression

$$y^2 = \frac{q}{m}\frac{B_0^2}{E_0}\frac{{L_{B1}}^2\left(L_{B1}/2+L_{B2}\right)^2}{L_{E1}\left(L_{E1}/2+L_{E2}\right)}\cdot x \qquad (1)$$

where E_0 and B_0 are the electric and magnetic fields, L_{B1}, L_{B2}, L_{E1} and L_{E2} are the dimensions of relevant sections of the TPS as labelled in Fig. 1. Since the locus of the parabolic ion traces produced by the TPS is a function of the charge-to-mass ratio (q/m) of the ion species, the traces of the species with the same q/m will overlap at the detector plane, preventing their spectra to be characterised. This is a fundamental limitation of a TPS when employed in high intensity laser plasma experiments, where several ion species around the interaction region are simultaneously accelerated to high energies [3, 4, 5], such as D^+, C^{6+} and O^{8+} (q/m=1/2).

Discrimination of light ions (such as D^+) can be achieved by filtering out the heavier one before reaching the detector. This is possible as all the ions in the same trace will have the same energy per nucleon at any given point of the trace, so heavier species can therefore be prevented from reaching the detector by exploiting differences in stopping power. However, using a metal foil with a single, fixed thickness in front of the detector may not be sufficient to recover the full D^+ spectrum, depending on the energy range covered by the TPS.

Here, we report on the characterisation of complete

spectrum of D^+ ions generated from a laser solid interaction by employing a differential filter (DF) over FUJI image plate detectors [6], which are commonly used in such experiments.

2 Experimental Setup

The experiment was carried out at the Rutherford Appleton Laboratory (RAL), STFC, UK by employing the petawatt arm of the VULCAN laser system. The data here presented were obtained by irradiating the laser onto 10 μm thick deuterated plastic (CD) foil targets. Using an $f/3$ off-axis parabolic mirror, the laser was focussed down to $\sim$ 6 μm full width at half maximum spots on the target, delivering peak intensity in excess of 10^{20} W cm^{-2}. The ions accelerated by the interaction of the intense pulse with the CD target were diagnosed by employing several TPSs, at different angles with respect to the laser axis.

The accelerated deuterium ions were discriminated from the heavier ones with the same q/m value (such as C^{6+}, O^{8+}, etc.) by using differential filtering in front of the detectors in each TPS. The DF (as discussed in section 3) was attached to a frame which was directly screwed onto the detector drum of the TPS, and served as a clamp to hold the detector plate (see Fig. 1). In this configuration the position of the DF always remains fixed with respect to the TPS, which is crucial for filtering ions in specific energy bands. BAS-TR imaging plates (IP) [6] were used as detectors. The IPs were wrapped with 6 μm thick Al foils to avoid their exposure to ambient light after irradiation.

3 Design of a Differential Filter (DF)

The design of a differential filter is based on using several filters of suitable materials and/or thicknesses in different regions of the detector, so for each zone, with boundaries defined by a pair of y coordinates (y_1, y_2), such a filter should be capable of stopping the heavier ions reaching the detector plane within this region.

It is to be noted that a DF has to be designed specifically for a given TPS and for the ion species under consideration, as those are the parameters that define the energy of the ions to filter at each point of the detector. Here we discuss filtering of C^{6+}, O^{8+} ions in order to obtain a clean track of D^+ on the detector. In the experiment, the TPS was set up (with B_0 = 0.988 T, E_0 = 11 kV/cm, L_{B1} = 50 mm, L_{B2} = 407 mm, L_{E1} = 150 mm, L_{E2} = 307 mm) to diagnose D^+ ions from $\sim$1 MeV/nucleon up to several tens of MeV/nucleon, spread over 55 mm along the energy dispersion axis of the detector. Considering the energy dispersion of the D^+ and C^{6+} ions, the 55 mm detection window was divided into 4 regions, where a suitable filter could be found for each region. The filter foils for each region were selected by considering the stopping power of both deuterium and carbon ions, obtained via SRIM simulations [7], as shown in Fig. 2.

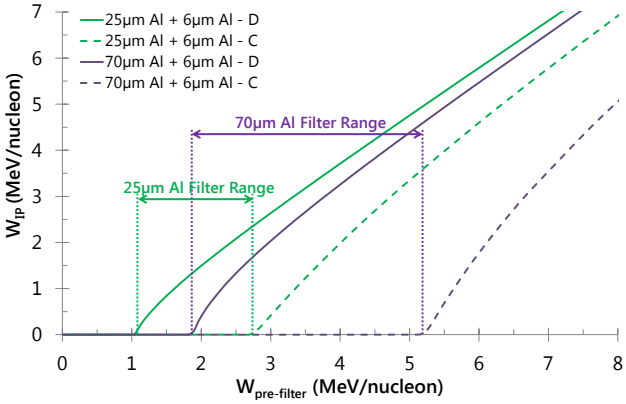

Figure 2: Graph showing incident vs. transmitted energies for deuterium (solid) and carbon (dashed) ions for 25 μm (blue) and 70 μm (red) aluminium foils, respectively, as obtained by SRIM [7] simulation. The ranges in which each filter was used are labelled. **(c)** Zoomed-in view of a small region in the data (as marked by dashed square in (b)) highlighting the abrupt increase in signal of 'D^+ track' and appearance of other ion species in the gap between two filter foils.

The choice of filter materials and thicknesses was simply based on their availability during the experiment. However, higher Z and thinner foils would be preferred in order to decrease lateral straggling of ions due to multiple small-angle scattering inside the filters, which may reduce the energy resolution of the diagnostic.

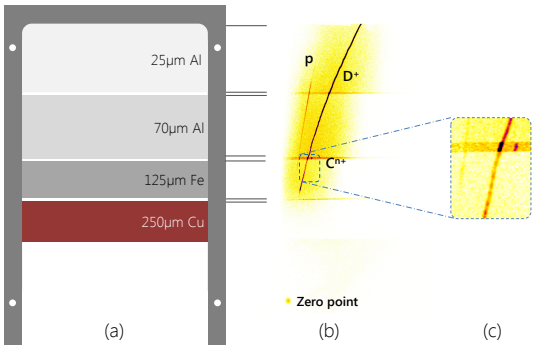

Figure 3: **(a)** Design of one of the DFs used in the experiment. **(b)** Typical raw data obtained in the experiment using the DF shown in (a). An abrupt increase in signal of 'D^+ track' and the appearance of other ion species can be seen in the gap between two filter foils.

A schematic of the DF used in the experiment is shown in the Fig. 3, along with typical data obtained in the campaign. The abrupt increase of the signal in the ion trace corresponding to q/m=1/2 and the appearance of other ion species tracks (such as C^{5+}, O^{7+}, etc.) in the gap between consecutive filter sheets (Fig. 3c) is evidence

of the effectiveness of the DF design used in the TPS for isolating deuterium ion spectra from the other ion species with the same q/m value.

4 Calibration of IP response to energetic deuterium ions

The calibration method, as used previously by several groups [8, 9], involves using CR-39 nuclear track detectors to compare the PSL signal obtained from the IP with the number of tracks produced in the CR-39. This method provides an absolute ion calibration, as each track produced in the CR-39 refers to a single ion. To obtain the IP response for a range of ion energies, a piece of CR-39 having closely spaced slots carved along the IP energy dispersion axis was placed in front of the IP [10]. The slotted CR-39 was used after the DF, ensuring that only the D^+ ions are exposed to the CR-39.

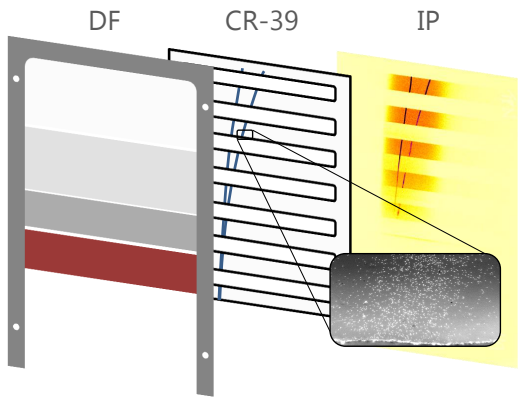

Figure 4: Example of the setup used for the BAS-TR IP calibration, showing experimental results from both the CR-39 detector and the image plate.

4.1 Track counting in CR-39

In order to develop the ion tracks for counting, the CR-39 pieces were etched in a 6M sodium hydroxide (NaOH) solution at a temperature of 85 ^{o}C. Etching was done for short periods of time (typically 5-10 mins), depending on the incident flux of particles on the CR-39, to avoid overlapping of ion tracks. Sets of pictures of the front surface of CR-39 were taken using an optical microscope with a 20× objective. The number of particle tracks at any given location was then counted by using the 'particle analysis' subroutine of ImageJ[11] software.

4.2 Estimation of IP signal incorporating PSL fading

The IPs were scanned using a commercial IP scanner (Fujifilm FLA-5000 [6]) with 16-bit dynamic range and 25 µm × 25 µm pixel size, which was converted from the scan value (or quantum level (QL)) to PSL using the formula given by the manufacturer [6]

$$PSL = \left(\frac{R}{100}\right)^2 \times \frac{4000}{S} \times 10^{L\times\left(\frac{QL}{2^G-1}-\frac{1}{2}\right)} \qquad (2)$$

where $R = 25$µm is the scanning resolution, $S = 5000$ is the sensitivity of the scanner, $L = 5$ is the latitude or level and $G = 16$ is the bit depth.

Due to the spontaneous decay of excited electrons from their metastable state, energy stored in the IP decays over time after the irradiation. As shown by several authors [9, 12] the fading of the IP signal can be described by different rates of decay, from a very fast decay over several tens of minutes after the irradiation to a significantly slower rate of decay lasting for days. The fading has usually been investigated by exposing the IP to radioactive sources (e.g. alpha, gamma) for a period of time ranging from few minutes to tens of minutes and scanning it after the exposure. Although this method is rigorous in describing the slow rate of decay, it does not allow sufficient accuracy for the measurement of the decay rate promptly after the irradiation. Moreover, the fading rate close to the time of irradiation can vary significantly depending on several factors such as the PSL signal strength at the time of exposure, duration of ionising radiation source, type of image plate, etc.

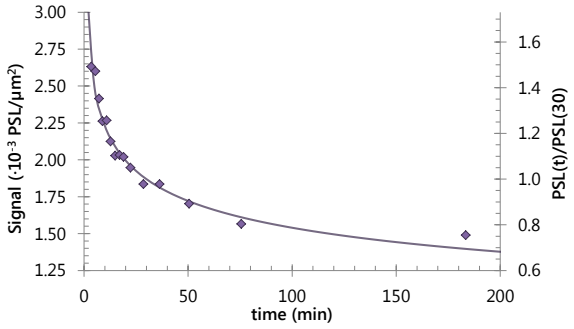

Figure 5: Experimentally measured PSL signal per unit area for different delayed scanning times are shown for the BAS-TR IP, while using 25×25µm scanning resolution. The solid line represents the fading curve, which is the best fit to the data points.

In order to overcome these factors, the decay characteristic of the BAS-TR image plate was studied experimentally by exposing the IP to a laser driven pulsed X-ray source of ns burst duration, employing TARANIS laser facility at the the Queen's University Belfast, UK. As shown in Fig. 5, PSL signal suffers a rapid decay in the first half hour after the exposure, followed by a significantly slower decay over several hours. Although the trend of the fading curve broadly matches the measurements taken by other groups (see the references [9, 12]), the agreement is best for long fading times of the order of hours.

Therefore, instead of obtaining a calibration curve in terms of PSL per ion at the time of exposure (i.e. t =

0), we choose to set the reference time at $t = 30$ minutes after irradiation, typical time required for retrieving the IPs from the vacuum interaction chamber. The PSL signal at the said reference point of time, i.e. 30 min. after exposure, can be estimated by the empirical formula

$$\mathrm{PSL}_{30} = \left(\frac{30}{t}\right)^{-0.161} \mathrm{PSL}(t) \tag{3}$$

where PSL(t) represents the measured PSL signal obtained from the IP scanned 't' minutes after the irradiation.

4.3 *Energy transmission*

As mentioned earlier, a calibration curve refers to the signal produced per ion as a function of ion energy per nucleon reaching the IP ($\mathrm{W_{IP}}$). Due to the use of the DF before the detectors in our case, the energy of deuterium ions incident on the IP/CR-39 at any given point of the ion track was different from that defined by the TPS energy dispersion. Therefore, for each data point obtained for the calibration curve, the energy of the D^+ ion on the image plate, after passing through the DF, was calculated by using SRIM simulation [7], as shown in Fig. 2 for the first two filter layers.

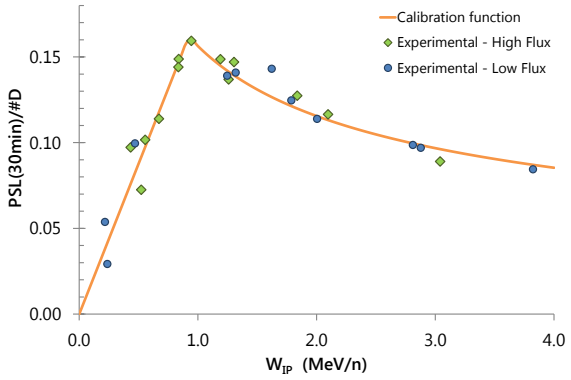

Figure 6: Absolute response of BAS-TR image plates to deuterium ions, correlating the PSL on the IP per incident D^+ ion for different D^+ energies on the IP.

Employing the methods discussed in the subsections A-C, the PSL_{30} per incident particle was obtained for several different D^+ energies at the IP, as shown in Fig. 6. The data points were divided into two groups depending on the signal strength, given by 0.02-0.08 PSL/μm^2 and 0.08-0.2 PSL/μm^2 in Fig. 6, corresponding to low and high particle fluxes($\sim$ 0.01 ions/μm^2 and a few ions/μm^2 respectively) on the detector. Both sets follow the same trend, which implies linear response of the IP with respect to the ion flux. In terms of ion energy, the PSL/particle for lower energy ions increases linearly with the incident ion energy, followed by a slower decay for higher energy ions. This behaviour of IP response can be crudely explained on the basis of the finite thickness of the IP active layer and the Bragg peak energy deposition process for ions. The empirical calibration function thus obtained as the best fit to the data points is given by Eq. 4.

$$\mathrm{PSL}_{30}/\mathrm{D}^+ = \begin{cases} 0.1754\ \mathrm{W_{IP}} & \mathrm{W_{IP}} < 0.931\ \mathrm{MeV/n} \\ 0.1563\ \mathrm{W_{IP}}^{-0.4363} & \mathrm{W_{IP}} \geq 0.931\ \mathrm{MeV/n} \end{cases} \tag{4}$$

where, $\mathrm{W_{IP}}$ represents the D^+ ion energy reaching the IP. Although Fig. 6 shows the calibration for D^+ ions with energies up to 4 MeV/nucleon, Eq. 4 can be used to obtain D^+ spectra up to significantly higher energies while using DF, as the DF tends to slow down the ions before reaching the IP.

5 Conclusions

In conclusion, a novel technique to obtain the spectrum of an ion species over a broad energy range by removing overlapping ion traces in Thomson parabola ion spectrometer is demonstrated. This method is based on differential filtering across the full range of energies produced, by which the lightest of the overlapping ions can be discriminated. The technique can also be applied for filtering proton track in a magnetic spectrometers, or, to filter high energy part of an ion spectrum in the region where several ion tracks are merged due to insufficient track separation. In addition to the D^+ spectrum obtained using DF, the BAS-TR image plate was absolutely calibrated for D^+ response against CR-39 detectors over a broad spectrum.

Acknowledgements

The authors acknowledge funding from EPSRC [EP/J002550/1-Career Acceleration Fellowship held by S. K., EP/L002221/1, EP/E035728/1, EP/K022415/1, EP/J500094/1 and EP/I029206/1], Laserlab Europe (EC-GA 284464), projects ELI (Grant No. CZ.1.05/1.1.00/483/02.0061) and OPVK 3 (Grant No. CZ.1.07/2.3.00/20.0279). Authors also acknowledge the support of the mechanical engineering staff of the Central Laser Facility, STFC, UK.

References

[1] Thomson, J. J., Proceedings of the Royal Society of London. Series A **89** (1913) 1.

[2] Gwynne, D. et al., Review of Scientific Instruments **85** (2014) 033304.

[3] McKenna, P. et al., Plasma Physics Controlled Fusion **49** (2007) B223.

[4] Kar, S. et al., Physical Review Letters **109** (2012) 185006.

[5] Jung, D. et al., New Journal of Physics **15** (2013) 123035.

[6] Fujifilm bas-tr imaging plates, `http://www.fujifilm.com`.

[7] Ziegler, J. F., Ziegler, M., and Biersack, J., Nuclear Instruments and Methods B **268** (2010) 1818 .

[8] Mori, M. et al., Plasma and Fusion Research **1** (2006) 042.

[9] Mancic, A., Fuchs, J., Antici, P., Gaillard, S., and Audebert, P., Review of Scientific Instruments **79** (2008) 073301.

[10] Prasad, R. et al., Nuclear Instruments and Methods in Physics Research Section A: Accelerators, Spectrometers, Detectors and Associated Equipment **623** (2010) 712.

[11] Imagej website, `http://rsbweb.nih.gov/ij/`.

[12] Paterson, I., Clarke, R., Woolsey, N., and Gregori, G., Measurement Science and Technology **19** (2008) 095301.